How time-discretization can break the asymptotics of inverse scattering *

Roel Snieder

Center for Wave Phenomena, Colorado School of Mines,
Golden CO 80401, USA,
email rsnieder@mines.edu

Abstract

Inverse scattering by the Marchenko or Gelfand-Levitan equations consists of two steps. The first step consists of solving an integral equation to retrieve the wavefield in the interior of a scattering medium from waves recorded outside of the scattering region. The second step consists of estimating the scattering potential from this wavefield. The estimation of the potential can be justified either by taking a high-frequency limit, or by evaluating the wavefield an infinitesimal time before or after the direct wave. Waveforms obtained in experiments are discretized in time with a sampling interval dt. We show an example that this time discretization precludes the extraction of the potential. The reason is that the frequencies of discretized waveforms are below the Nyquist frequency. This limitation precludes taking the high-frequency limit that is used for estimating the potential from the waveforms in the interior of the scattering region. We present an alternative method to estimate the potential from wave fields in the interior of the scattering region. This method can be used even when the waves are in the strong scattering regime.

Keywords: inverse scattering, imaging, Marchenko

1 Introduction

Inverse scattering methods, where medium properties are computed in an exact way from recorded scattering data have been formulated the Schrödinger equation in one dimension or for radially symmetric potentials [1, 2, 3]. A comprehensive overview of inverse scattering for such systems has been given by Chadan and Sabatier [4], and the extension to three-dimensional system is described by Newton [5]. These inverse scattering techniques have

*This paper is published as: Snieder, R., 2023, How time-discretization can break the asymptotic of inverse scattering, *Proc. Roy. Soc. A* **479**: 20230711, https://doi.org/10.1098/rspa.2023.0177

been generalized to scattering in a layered acoustic medium [6], to the plasma wave equation and to scattering of acoustic waves in a duct with variable area [7].

The inverse scattering methods are exact, and the model reconstruction consists of two steps. The first step is to solve an integral equation, such as a the Marchenko equation or the Gelfand-Levitan equation, to provide the wavefield in the interior of the scattering region from recorded scattering data. This step amount to a continuation of the wavefield recorded at a boundary into the unknown interior of the medium. The second step consists of estimating the potential from the wavefield in the interior [7]. The second step of estimating the potential involves asymptotics, and there are different ways to derive this step. The derivation sketched by Faddeev [3] is based on an integral equation of the wavefield, and one takes a combination of spatial and temporal derivatives at a time just after the arrival of the direct wave. When the direct wave arrives at a time t_d, this involves a limit $t \to t_d$. The derivation of Burridge [7] is based on a Taylor expansion of the wavefield for times close to the arrival time of the direct wave, and also takes the limit $t \to t_d$.

In practice, scattering data recorded in the time domain are discretized with a finite sampling time dt. This means that one cannot take the limit $t \to t_d$, because the smallest resolvable difference between the time t is and the arrival time t_d of the direct wave is given by the sampling time dt. We show that this limitation may make it impossible to accurately reconstruct the potential from the wavefield in the interior based on the reconstruction algorithm proposed by Burridge [7].

In this paper we follow the analysis of Burridge [7] and consider the plasma wave equation in one dimension

$$u_{xx}(x,t) - \frac{1}{c_0^2} u_{tt}(x,t) - q(x)u(x,t) = 0 \ , \tag{1}$$

where the subscript x or t denotes the x and t-derivatives respectively. We assume that the velocity c_0 is constant. Section 2 features the derivation by Burridge [7] to estimate the potential from the wavefield in the interior. We show in section 3 that one can estimate the wavefield in the interior from scattering data using recent techniques for Green's function retrieval. To ensure that problems with reconstruction of the potential are not caused with difficulties in estimating the wavefield inside the scatterer, we present in section 4 the analytical expressions for the wavefield inside a block potential. The corresponding time-domain waveforms are shown in section 5, and we show the difficulty of estimating the potential by applying the asymptotic relation of Burridge [7] to wave fields that are discretized in time in section 6. The inability to estimate the potential from discretized data using the asymptotic relations from Burridge [7] does not mean that the potential cannot be estimated. We provide an alternative method to estimate the potential from the wavefield inside the scatterer in section 7. This method is exact, it can be applied to data that are discretized in time, and it does not matter where the scattering is weak or strong.

2 The discontinuity in the wavefield after the wavefront and q.

In this section we show the derivation of Burridge [7] to retrieve the potential $q(x)$ from the wavefield inside the medium from the value of the wavefield just after the direct wave.

We assume that this wavefield is estimated from one of the inverse scattering methods as described by Burridge [7].

Consider a solution $u(x,t)$ of the plasma wave equation (1). Following the treatment Burridge [7] we use a set of functions $f_n(t)$ that are defined recursively by

$$f_n(t) = \int_{-\infty}^{t} f_{n-1}(t) \; . \tag{2}$$

The recursion starts with

$$f_0(t) = \delta(t) \; , \tag{3}$$

with $\delta(t)$ the Dirac delta function. Integrating the recursion (2) with the starting value (3) gives for $n \geq 1$:

$$f_n(t) = \frac{1}{(n-1)!} t^{n-1} H(t) \; , \tag{4}$$

where $H(t)$ is the Heaviside function. Taking the time derivative of expression (2) implies that

$$\dot{f}_n(t) = f_{n-1}(t) \; . \tag{5}$$

The functions $f_n(t)$ describe the properties of the wavefield at times close the arrival of the direct wave. Assuming infinite bandwidth, the lowest order contribution $f_0(t) = \delta(t)$ gives the wavefield of the ray-geometric wavefield on the wavefront. The function $f_1(t) = H(t)$ gives the constant component of the wavefield just after the direct arriving waves. The higher order $f_n(t)$ account for a power series expansion of the wavefield after the direct arriving wave. For a Fourier transform $f(t) = \int F(\omega) \exp(-i\omega t) d\omega$, the recursion (5) corresponds to $F_n = F_{n-1}/(-i\omega)$. An expansion in functions $f_n(t)$ in the time domain thus corresponds to an expansion in $1/(-i\omega)^n$ in the frequency domain. The expansion is explained in more detail in section 5.6.5 of Červený [8].

Next expand the wavefield in a series of the $f_n(t)$

$$u(x,t) = \sum_{n=0}^{\infty} a_n(x) f_n(t - \tau(x)) \; , \tag{6}$$

where the travel time $\tau(x)$ is not yet specified. The restriction $n \geq 0$ is incorporated in the following by setting

$$a_n(x) = 0 \quad \text{for} \quad n < 0 \; . \tag{7}$$

Note that the $a_n(x)$ depend on space only.

Taking the second x-derivative of the expansion (6), while using the property (5) in the derivatives gives

$$u_{xx}(x,t) = \sum_n \left(a_n \tau_x^2 f_{n-2} - \left(a_n \tau_{xx} + 2 \frac{\partial a_n}{\partial x} \tau_x \right) f_{n-1} + \frac{\partial^2 a_n}{\partial x^2} f_n \right) \; , \tag{8}$$

where for brevity we omit the arguments of $a_n(x)$ and $f_n(t - \tau(x))$. Replacing $n \to n-1$ in the second term and $n \to n-2$ in the last term gives

$$u_{xx}(x,t) = \sum_n \left(a_n \tau_x^2 - \left(a_{n-1} \tau_{xx} + 2 \frac{\partial a_{n-1}}{\partial x} \tau_x \right) + \frac{\partial^2 a_{n-2}}{\partial x^2} \right) f_{n-2} \; . \tag{9}$$

Applying this treatment to all the terms in the plasma wave equation (1) gives

$$\sum_n \left(\left(\tau_x^2 - \frac{1}{c_0^2} \right) a_n - \left(a_{n-1}\tau_{xx} + 2\frac{\partial a_{n-1}}{\partial x}\tau_x \right) + \left(\frac{\partial^2 a_{n-2}}{\partial x^2} - q a_{n-2} \right) \right) f_{n-2} = 0 \ . \tag{10}$$

Consider the first term $n = 0$ in the series (10). Since $a_n = 0$ for $n < 0$, the $n = 0$ contribution to expression (10) reduces to $(\tau_x^2 - 1/c_0^2)\, a_0 = 0$. For nontrivial solutions $a_0 \neq 0$, this implies that $\tau(x)$ satisfies the eikonal equation:

$$\tau_x^2 = \frac{1}{c_0^2(x)} \ . \tag{11}$$

For a rightgoing wave that passes the origin $x = 0$ at $t = 0$,

$$\tau(x) = x/c_0 \ , \tag{12}$$

and therefore

$$\tau_x = 1/c_0 \quad \text{, and} \quad \tau_{xx} = 0 \ . \tag{13}$$

The expressions (12) and (13) reduce the series (10) to

$$\sum_n \left(\frac{2}{c_0}\frac{\partial a_{n-1}}{\partial x} + \left(\frac{\partial^2 a_{n-2}}{\partial x^2} - q a_{n-2} \right) \right) f_{n-2} = 0 \ . \tag{14}$$

Consider next the term $n = 1$ to this series. Since a_{-1} vanishes, the $n = 1$ contribution to the series can vanish only when $\partial a_0/\partial x = 0$. Assuming the incoming wave has a unit amplitude, which implies that

$$a_0(x) = 1 \ . \tag{15}$$

To retrieve the potential q set $n = 2$ in expression (14) and insert equation (15), which gives

$$q(x) = -\frac{2}{c_0}\frac{\partial a_1}{\partial x} \ . \tag{16}$$

Expression (16) gives q in terms of the coefficient a_1. The amplitude $a_1(x)$ cannot assumed to be known, because the inhomogeneous medium is not know. But if we know the wavefield inside the inhomogeneous medium, we can express $a_1(x)$ in this wavefield. Using equations (3) and (4) one can write expression (6) as

$$u(x,t) = u_0(x,t) + a_1(x)H(t - x/c_0) + \sum_{n=2}^{\infty} \frac{a_n(x)}{(n-1)!}(t - x/c_0)^{n-1} H(t - x/c_0) \ . \tag{17}$$

In this expression the unperturbed wave in the reference medium is given by

$$u_0(x,t) = \delta(t - x/c_0) \ . \tag{18}$$

Next evaluate equation (17) at an infinitesimal time $t = x/c_0 + \varepsilon$ just after the arrival time of the direct wave, and take the limit $\varepsilon \downarrow 0$. Because of the terms $(t - x/c_0)^{n-1}$ the terms in

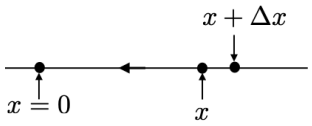

Figure 1: Definition of the coordinates used to estimate the Green's function

the sum in expression (17) vanish in this limit, and $H(t - x/c_0) = 1$ in this limit. Following expression (18), $u_0(x, t = x/c_0 + \varepsilon) = \delta(\varepsilon) = 0$. This means that

$$a_1(x) = \lim_{\varepsilon \downarrow 0} u(\mathbf{r}, t = x/c_0 + \varepsilon) \; . \tag{19}$$

With expression (16) this implies that the potential is equal to the derivative of the wavefield just after the direct wave

$$q(x) = -\frac{2}{c_0} \lim_{\varepsilon \downarrow 0} \frac{\partial u(x, t = x/c_0 + \varepsilon)}{\partial x} \; . \tag{20}$$

This expression is similar to potential retrieved for the three-dimensional Marchenko equation derived by Newton [9] where the potential is also given by the derivative of the wavefield just after the direct wave.

3 Retrieving the potential from inverse scattering data

Expression (20) shows that the potential is known if one knows the wavefield inside the potential just after the time of the direct wave. This replaces the determination of the potential with the determination of the wavefield in the interior from scattering data. The crux of inverse scattering methods is that these algorithms allow us to determine the wavefield in the interior of a medium from scattering data recorded at the boundary, without knowing the potential. Burridge [7] provides several examples of this principle, and he shows that one can, in fact, retrieve different wavefield solutions in the interior that satisfy different causality properties.

In the following we use, for the sake of argument, inverse scattering solutions that provide the Green's function for a source point inside the medium. The focusing of the wavefield in an unknown medium using was formulated by Rose [10, 11, 12]. Since the focused wavefield corresponds to the Green's function, the used inverse scattering methods give the Green's function for a source point inside the unknown one-dimensional medium [13]. The principle of Green's function retrieval has been extended to more space dimensions [14, 15]. These methods rely on the Marchenko equations in one or more dimensions.

In the following we assume that we have retrieved the Green's function $G(x = 0, x, t)$ for a source point x in the interior of the medium that is recorded at the boundary $x = 0$, see Figure 1. Since the point x can be arbitrarily chosen, one can also retrieve the Green's function $G(x = 0, x + \Delta x, t)$ for a nearby point. Because of reciprocity [16], these Green's functions are equal to $G(x, x = 0, t)$ and $G(x + \Delta x, x = 0, t)$, respectively. These Green's

functions describe the wavefield excited by a point source at $x = 0$ at the points x and $x+\Delta x$, respectively. This provides us with the wavefield in the interior at two adjacent points, and by computing the x-derivative by differencing these wavefields and letting $\Delta x \to 0$ and can then retrieve the potential from expression (20). We illustrate this procedure, and it's limitations with a numerical example based on an analytical expression for the wavefield instead of the wavefield reconstructed with one of the integral equations of inverse scattering. This ensures that an inability to retrieve the potential is due to the estimation of expression (20).

4 Scattering for a block potential

As an example of the reconstruction of the potential from wavefields, consider the special case of a block potential that is only nonzero for $0 < x < L$:

$$q(x) = \begin{cases} Q & \text{for } 0 < x < L \\ \\ 0 & \text{for } x < 0 \text{ or } x > L \end{cases} \tag{21}$$

In the following we determine the wavefield in the frequency domain for angular frequency ω for an incident unit wave from the left. This wavefield is given by

$$u(x) = \begin{cases} e^{ik_0 x} + Re^{-ik_0 x} & \text{for } x < 0 \,, \\ \\ Ae^{ikx} + Be^{-ikx} & \text{for } 0 < x < L \,, \\ \\ Te^{ik_0 x} & \text{for } L < x \,, \end{cases} \tag{22}$$

where

$$k_0 = \frac{\omega}{c_0} \,, \tag{23}$$

and

$$k = \sqrt{\frac{\omega^2}{c_0^2} - Q} \,. \tag{24}$$

The reflection coefficient R, the transmission coefficient T and the constants A and B follow from the requirements that u and $\partial u/\partial x$ are continuous at $x = 0$ and $x = L$. This gives four equations that allow the coefficients A, B, R, and T to be computed recursively from the following expressions:

$$Det = (k + k_0)^2 e^{-ikL} - (k - k_0)^2 e^{ikL} \,, \tag{25}$$

$$A = 2k_0(k + k_0)e^{-ikL}/Det \,, \tag{26}$$

$$B = 2k_0(k - k_0)e^{ikL}/Det \tag{27}$$

$$R = A + B - 1 \,, \tag{28}$$

$$T = \left(Ae^{ikL} + Be^{-ikL}\right) e^{-ik_0 L} \,. \tag{29}$$

These coefficients can be computed for every angular frequency and with expression (22) gives the wavefield as a function of position and frequency. A Fourier transform then gives the waveform in the time-domain.

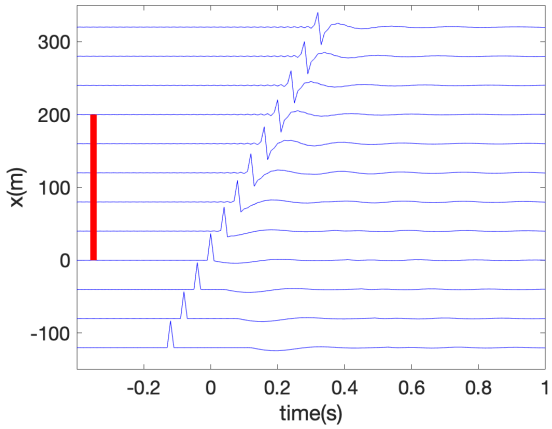

Figure 2: Time-domain waveforms for the block potential for $Q = 0.001\ m^{-2}$. The incident wave is a delta function discretized with the time interval $dt = 0.01\ s$. The red bar gives the spatial extent of the block potential.

5 A numerical example of waveforms

In this section we show numerical examples of time-domain waveforms for the block potential. We use parameters that are representative of a seismic experiment. The time-domain waveforms are discretized with a time interval $dt = 0.01\ s$. Each time series has $N = 1024$ samples and the background velocity is $c_0 = 1000\ m/s$. The potential is nonzero over and interval $L = 200\ m$.

Figure 2 shows the waveforms when $Q = 0.001\ m^{-2}$. A delta function is incident from the left. Since the time series is discretized, the incident delta function is discretized as well. As the incident wave propagates through the block potential from $x = 0\ m$ to $x = 200\ m$ the amplitude of the direct wave slowly decreases and a negative sidelobe forms just after the direct wave. A weak reflected wave arrives at the lowest trace at around $t = 0.2\ s$.

Figure 3 shows time-domain waveforms for $Q = 0.01\ m^{-2}$. Just like in the previous example a delta function is incident from the left. Once this wave enters the potential at $x = 0\ m$, it looses its character as a delta function and the direct propagating wave is dispersive with high frequencies arriving before the lower frequencies arrive. A pronounced low-frequency reflected wave is reflected from the left edge of the block potential at $x = 0$.

The direct wave in the block potential is dispersive. For a fixed angular frequency ω the direct wave is given by $\exp(ikx - \omega t)$. Inserting this in the plasma wave equation (1) gives within the block potential where $q(x) = Q$ the dispersion relation

$$k^2 = \frac{\omega^2}{c_0^2} - Q\ . \tag{30}$$

The phase velocity follows the relation $C = \omega/k$ and the group velocity from $U^{-1} = \partial k/\partial\omega$,

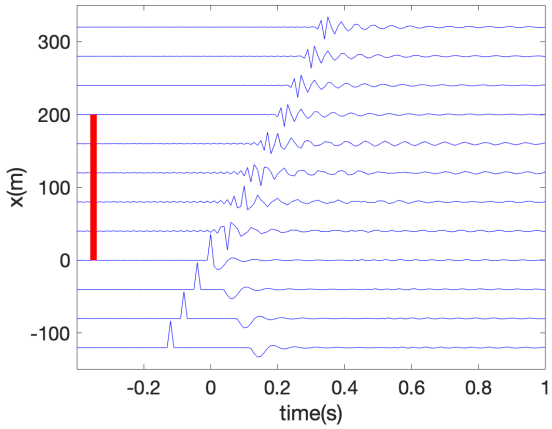

Figure 3: Time-domain waveforms for the block potential for $Q = 0.01\ m^{-2}$. The incident wave is a delta function discretized with the time interval $dt = 0.01\ s$. The red bar gives the spatial extent of the block potential.

these velocities are given by

$$C = \frac{c_0}{\sqrt{1 - \dfrac{Qc_0^2}{\omega^2}}}\ , \tag{31}$$

and

$$U = c_0\sqrt{1 - \frac{Qc_0^2}{\omega^2}}\ . \tag{32}$$

For $Q > 0$, the group velocity increases with frequency so that the high frequency waves arrive before the low frequency waves, this indeed happens in Figure 3. For frequencies $\omega \gg Qc_0^2$ the dispersion is negligible. It follows from the dispersion relation (30) that k^2 is negative when $\omega < Qc_0^2$, which means that the wavefield is evanescent for these angular frequencies. We define an critical angular frequency $\omega_c^2 = Qc_0^2$ that corresponds to a critical frequency

$$f_c = \frac{\sqrt{Q}c_0}{2\pi}\ . \tag{33}$$

The wavefield is propagating when $f > f_c$ and it is evanescent when $f < f_c$. For $f \gg f_c$ the dispersion is negligible.

The concept of the critical frequency allows us to explain the quantitative difference in the waveforms in Figures 2 and 3. For both figures a sampling interval $dt = 0.01\ s$ is used. This sampling interval implies that the discretized waveforms only contain frequency components up to the Nyquist frequency [17] that is given by

$$f_N = \frac{1}{2dt}\ . \tag{34}$$

For the used sampling interval, the Nyquist frequency in both waveforms is this equal to 50 Hz.

Table 1: The critical frequency f_c and the Nyquist frequency f_N for different values Q of the block potential.

	$Q = 0.001\ m^{-2}$	$Q = 0.01\ m^{-2}$
f_c	5 Hz	16 Hz
f_N	50 Hz	50 Hz

Table 1 gives the critical frequency and the Nyquist frequency for the two waveform examples. For Figure 2 the Nyquist frequency is 10 times as large as a the critical frequency. Most of the frequency components in the waveforms thus are above the critical frequency and there is little dispersion. Note however, that the amplitude of the direct wave decreases as the wave propagates through the block potential. This is due to frequency component $f < f_c$ that are evanescent with the block potential.

As shown in Table 1, the critical frequency in the example of Figure 3 for $Q = 0.01\ m^2$, a third of the frequency components are below the critical frequency ($f < f_c$). The waves at these frequencies are evanescent, hence the amplitude of the transmitted waves. In addition, since the critical frequency f_c is only about 30% of the Nyquist frequency f_N, the dispersion in the direct wave in appreciable.

If the waves would have have infinite bandwidth, the time-domain waveforms would not be disturbed strongly by the potential because most frequencies would be above the critical frequency f_c. There would be little dispersion, and only a small fraction of the frequency components would be evanescent. In that case the direct wave would be well-described by a delta function with constant amplitude, as is the case in expression (18) that follows from the asymptotic analysis of Burridge [7]. This asymptotic analysis corresponds to a high-frequency approximation. But for discretized time series the frequencies are limited by the Nyquist frequency , $f \leq f_N$, and as shown in Table 1 the critical frequency f_c is in he numerical examples appreciable compared to the Nyquist frequency f_N. This raises the question to what extent the asymptotic analysis of section 2 is applicable to the waveforms in Figures 2 and 3, and to what extent the potential can be retrieved from expression (20).

6 Retrieving the potential from expression (20)

In this work we use the exact solution (22) of the wavefield instead of a wavefield estimate obtained from scattering data with the Marchenko equation. By using the exact wavefield, we can be assured that any discrepancies between the true potential and the estimated potential are due to the estimation of the potential from the wavefield, but that these discrepancies are not due to inaccuracies in the estimation of the wavefield inside the medium.

We retrieve the potential from the waveforms in Figure 2 using expression (20). In this example we used a space discretization $dx = c_0 dt = 10\ m$ to ensure that the direct wave arrives at a grid point. The direct waves arrives at time $t = x/c_0$, hence the wavefield just after the direct wave arrives at the next discretized time $t = x/c_0 + dt$, giving the wavefield $u(x, t = x/c_0 + dt)$. Replacing the x-derivative by a finite difference derivative, the discretized

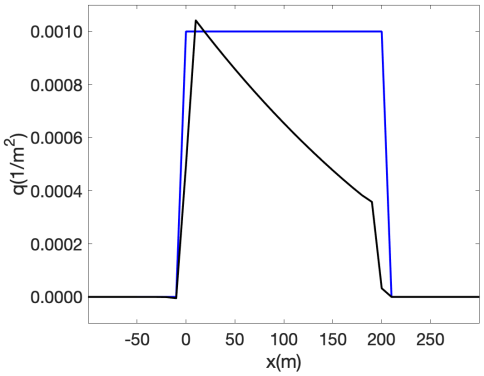

Figure 4: Black line: the potential estimated by applying the expression (35) to the waves in Figure 2. The true potential is shown with blue line.

form of equation is given by

$$q_{est} = -\frac{2}{c_0} \frac{u(x+dx, t=(x+dx)/c_0+dt) - u(x, t=x/c_0+dt)}{u_{max}\ dtdx} \ . \tag{35}$$

The factor dx in the denominator comes from the finite difference used to estimate the x-derivative in expression (20). In the treatment of section 2 the incident wave is according to expression (18) is a delta function in time, hence $\int u_0(x,t)dt = \int \delta(t - x/c_0)dt = 1$. In the numerically computed wavefield in Figure 2 the incident wave for $x < 0$ has a maximum amplitude u_{max} at its peak. The integrated value of this incident wave is $u_{max}dt$, and we normalized expression (35) with this factor to ensure that the wavefield is normalized in the same way as in the asymptotic treatment of section 2.

The potential retrieved from the waveforms in Figure 2 from expression (35) is shown by the black line in Figure 4. The true potential, for $Q = 0.001\ m^{-2}$ is shown by the black line. The left flank of the potential is estimated well, but for increasing values of x the estimated potential is smaller than the real potential. As argued before, for frequencies $f < f_c$ the wavefield in evanescent in the block potential. In addition, part of the directed wave is reflected off the left side of the block potential. The direct wave in expression (18) of the asymptotic treatment of section 2 ignored the reflection losses and reduction in amplitude due to evanescence. Yet the direct wave in Figure 2 is reduced in amplitude as it propagates through the block potential. This reduction in amplitude of the local direct wave also causes a loss in amplitude in the wavefield just after the direct wave, and a as result expression (35) underestimates the reconstructed potential.

The main flaw of the asymptotic treatment of section 2 is that the used asymptotic treatment implicitly invokes a high-frequency approximation ($f \rightarrow \infty$). For discretized time series the frequency is limited by the Nyquist frequency ($f \leq f_N$), and therefore the asymptotic treatment may not be accurate for these discretized time series. This deviation from the asymptotic treatment in section 2 is even more apparent for the waveforms in Figure 3 for the case $Q = 0.01\ m^{-2}$. In this case there is no clear direct wave that resembles the asymptotic direct wave of expression (18). The dispersive direct wave in Figure 3 does not

resemble a delta function at all, and it is not possible to identify the wavefield one sample after the arrival of this direct wave as used in the reconstruction equation (35). The recipe for the reconstruction of the potential of Burridge [7] is thus not applicable to this discretized time series.

7 Estimating the potential from full wave solutions

Next, I present an alternative method to estimate the potential from the wavefield obtained from solving inverse scattering equations, such as the Marchenko equation. We assume that we have reconstructed the wavefield in the interior of the potential. Instead of the estimating the potential from expression (20) that is based on asymptotics, we suggest a simple alternative: insert the wavefield in the wave equation (1) and solve for the potential, this gives:

$$q(x) = \frac{u_{xx}(x,t) - c_0^{-2} u_{tt}(x,t)}{u(x,t)} \ . \tag{36}$$

For every location x this equation provides a constraint for every time t. This approach has two complications. The resulting system is overdetermined, which can be remedied by solving the equations in the least-squares sense. As shown in the example in Figures 2 and 3, the wavefield is zero, or close to zero for many times t. For such times the ratio in expression (36) is unstable.

These complications can both be handled by multiplying the wave equation (1) with $u(x,t)$, integrating over time, and solving for $q(x)$, this gives

$$q(x) = \frac{\int u(x,t) u_{xx}(x,t) dt - c_0^{-2} \int u(x,t) u_{tt}(x,t) dt}{\int u^2(x,t) dt + \varepsilon} \ . \tag{37}$$

This is a single equation and is hence not overdetermined. The multiplication with $u(x,t)$ down-weights the contribution of times when the wavefield is small. In principle one can use any time interval for expression (37). One could also include a weight function in time integration. The integral $\int u^2(x,t) dt$ in the denominator is non-negative. For values of x where this integral is small the solution can stabilized with the regularization parameter ε in the denominator.

In the numerical example in this section, we estimate the second space derivatives with the simplest centered estimator $f_{xx} = (f_{i+1} - 2f_i + f_{i-1})/(dx)^2$, where f_i denotes the function at space discretization point i, and use a similar estimator for the second time derivative. Higher order estimators can improve the accuracy at the expense of reducing spatial resolution. One cannot apply expression (37) with this estimators to the waveforms in Figures 2 and 3 because the delta functions in these waveforms are not handled accurately by these estimators of the second derivative.

This complication can be avoided by convolving the waveforms with a wavelet that effectively applies a low-pass filter to the waveforms. Figure 5 show the waves in Figure 2 after convolution with a Ricker wavelet [18]. This wavelet is in the frequency domain given by

$$W(f) = \left(\frac{f}{f_R} \right)^2 \exp\left(-(f/f_R)^2 \right) \ . \tag{38}$$

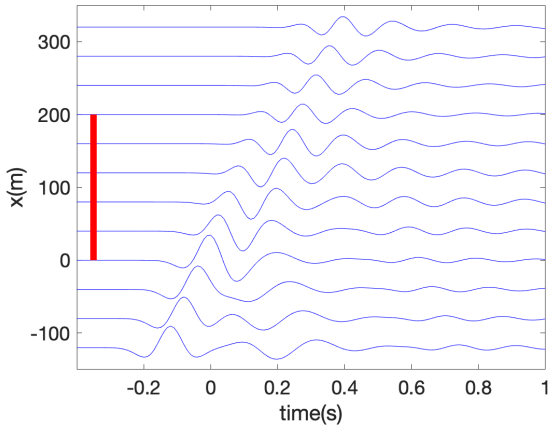

Figure 5: Time-domain waveforms for the block potential for $Q = 0.001\ m^{-2}$ after convolution with a Ricker wavelet that in the frequency domain is given by equation (38) for $f_R = 5\ Hz$. The red bar gives the spatial extent of the block potential.

In this example we used the value $f_R = 5\ Hz$. Note that in contrast to the unfiltered data in Figure 2, the filtered data in Figure 5 show strong reflected waves and reverberations in the block potential. This is due to the fact that the peak frequency of the Ricker wavelet $f_R = 5\ Hz$ is equal to the critical frequency, see Table 1. The filtered waveforms are the in the strong scattering regime, but since the estimator (37) is exact, at least for $\varepsilon = 0$, it does not matter when the waves are weakly to strongly influenced by the potential.

The potential estimated by applying equation (37) to the filtered waveforms of Figure 5 is shown by the blue line in Figure 6. The true potential is shown by the black line. In this section the regularization parameter ε is rather arbitrarily set to 1% of the the maximum of $\int u^2(x,t)dt$ for all values of x. The potential is reconstructed well. The edges of the block potential are not quite vertical, this is due to the used estimator for the second derivative with the used spatial sampling $dx = 10\ m$. The regularization causes the potential to be slightly underestimated. Without the regularization ($\varepsilon = 0$) some weak oscillations show up for $x \approx -50\ m$.

Figure 7 show the estimated potential by applying the same procedure to the wave in Figure 3 for the more strongly scattering case $Q = 0.01\ m^{-2}$. Note that the potential is also reconstructed well, although the regularization caused a more pronounced underestimation of the potential than in Figure 6. Note that the potential is retrieved from the dispersive waveforms in Figure 3 that precluded estimating the potential from expression (20). In contrast, the estimator (37) can be applied to waveforms of any complexity. For this example the frequency of the Ricker wavelet ($f_R = 5\ Hz$) is significantly less than the critical frequency for this potential ($f_c = 16\ Hz$). The filtered data are thus strongly scattered, but the estimated potential is retrieved quite well.

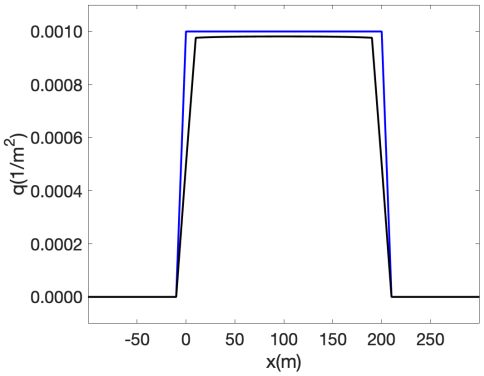

Figure 6: Black line: the potential estimated by applying the expression (37) to the filtered waves in Figure 5 for $Q = 0.001\ m^{-2}$. Blue line: the true potential.

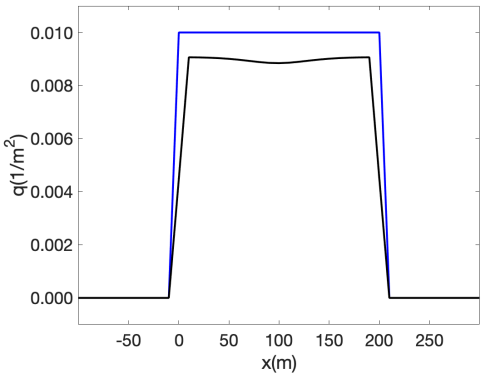

Figure 7: Black line: the potential estimated by applying the expression (37) to the waves in Figure 3 for $Q = 0.01\ m^{-2}$ after convolution with the Ricker wavelet. Blue line: the true potential.

8 Conclusion

In practice, recorded waveforms are discretized in time. For a sampling time dt this limits the frequencies in the digitized waveforms to frequencies less or equal than the Nyquist frequency $f \leq f_N = 1/(2dt)$. The asymptotic recovery of the potential proposed by Burridge [7] implicitly involves a high-frequency limit $f \to \infty$. We show an example that the limitation of the frequency band to the Nyquist frequency may preclude the extraction of the potential from discretized waveforms. Another way to view this inability is that the extraction of the potential depends on the wavefield an infinitesimal time after the direct wave [7, 3]. For discretized waveforms one may not be able to evaluate the wavefield just after the direct wave because the shortest time interval that can be resolved for discretized waveforms is the sampling time dt.

However, one can still use inverse scattering based on the Marchenko or the Gelfand-Levitan equations and estimate the medium properties without using the asymptotics used in inverse scattering methods [7]. One approach, which is used in seismic imaging, is to use the Marchenko equation to redatum recorded seismic waves from the surface to upgoing and downing waves on a prescribed reference depth in the subsurface [14, 15]. Using multidimensional deconvolution, these upgoing and doing waves can be used to compute the reflectivity of the subsurface under the redatuming level, and standard imaging can then be used to determine an image of the subsurface below the redatuming level [19, 20, 21].

I propose an alternative method to extract the potential. The first step consists of using the Marchenko or the Gelfand-Levitan equations to compute a wavefield in the interior of the medium using one of the methods described by Burridge [7]. In principle one can determine the potential by inserting this wavefield into the plasma wave equation (1) and solve for the potential $q(x)$, see expression (36). This leads, however, to an overdetermined system because for every location x one knows the wavefield of many times t. In addition, solving for the potential involves division by $u(x,t)$, which gives instabilities when the wavefield vanishes or is small compared to noise levels. We propose to retrieve the wavefield from expression (37) obtained by multiplying the plasma wave equation (1) with $u(x,t)$, integrating over time, and solving the result for $q(x)$. The numerical examples in the Figures 6 and 7 show that this leads to a stable estimation of the potential. This approach does not depend on a linearization between the wavefield and the potential, as is used implicitly in the asymptotics used by Burridge [7]. In fact, in the examples of Figures 6 and 7, the wavefield is restricted to contain mostly frequencies less that 5 Hz, whereas according to Table 1, the critical frequencies f_c are equal to 5 Hz and 16 Hz, respectively. This means that the waveforms used for the reconstruction of the potential in Figures 6 and 7 is in the multiple scattering regime.

The fact that the potential has been estimated well in Figures 6 and 7 does not mean that one can always estimate the potential accurately. When the potential is so strong that waves are evanescent, one can still use the Marchenko equation to determine the wavefield in the interior of the medium [22], but when the waves are damped to strongly that they are comparable to the numerical or experimental noise level, the extracted potentials cannot be estimated in a stable way [23, 24].

Generalizing the proposed methodology to more general realistic inverse scattering problem requires further research. For acoustic waves, the wave equation depends on the mass

density ρ and the compressibility κ. In this case one thus needs to invert for two unknown parameters, hence one needs two equations. This can, in one dimension, be achieved by reconstructing both the density p and the longitudinal component v of the velocity, and by retrieving the density and velocity from the equation of motion and the constitutive equation, respectively. Furthermore, inverse scattering in more than one dimension requires knowledge of the reflected waves and a smooth background model for the velocity [25, 14]. One thus needs to disentangle the smooth velocity variations from short-scale velocity variations. In reconstructing the Green's function by inverse scattering, one has a choice whether to estimate the full Green's function, the Green's function of the scattered waves, or the linearized Green's function, and one can exploit these different approached for medium estimation, especially when one considers an alternative approach to estimate the medium properties from the Lippman-Schwinger instead of the wave equation [26]. The strategy to estimate medium properties from reconstructed wavefields thus has many open research questions.

Acknowledgement: This research was supported by the Consortium Project on Seismic Inverse Methods at the Center for Wave Phenomena, Colorado School of Mines.

References

[1] V.A. Marchenko. The construction of the potential energy from the phases of scattered waves. *Doklady Akademii Nauk*, 104:695–698, 1955.

[2] Z.S. Agranovich and V.A. Marchenko. *The Inverse Problem of Scattering Theory*. Gordon and Breach, New York, 1963.

[3] L.D. Faddeev. Inverse problem of quantum scattering theory. II. *J. of Soviet Math.*, 5:334–396, 1976.

[4] K. Chadan and P.C. Sabatier. *Inverse Problems in Quantum Scattering Theory*. Springer-Verlag, second edition, 1989.

[5] R.G. Newton. *Inverse Schrödinger Scattering in Three Dimensions*. Springer Verlag, Berlin, 1989.

[6] R.G. Newton. Inversion of reflection data for layered media: A review of exact methods. *Geophys. J.R. Astron. Soc.*, 65:191–215, 1981.

[7] R. Burridge. The Gel'Fand-Levitan, the Marchenko and the Gopinath-Sondi integral equations of inverse scattering theory, regarded in the context of the inverse impulse response problems. *Wave Motion. An International Journal Reporting Research on Wave Phenomena*, 2:305–323, 1980.

[8] V. Červený. *Seismic Ray Theory*. Cambridge University Press, Cambridge UK, 2001.

[9] R.G. Newton. Inverse scattering II, three dimensions. *Journal of Mathematical Physics*, 21:1698–1715, 1980.

[10] J.H. Rose. Single-sided autofocusing of the of time-dependent Schrödinger equation. *Physical Review A: Atomic, Molecular, and Optical Physics*, 65:012707, 2001.

[11] J.H. Rose. Single-sided autofocusing of sound in layered materials. *Inverse Problems. An International Journal on the Theory and Practice of Inverse Problems, Inverse Methods and Computerized Inversion of Data*, 18:1923–1934, 2002.

[12] J.H. Rose. Single-sided focusing and the minimum principle of inverse scattering theory. *Inverse Problems. An International Journal on the Theory and Practice of Inverse Problems, Inverse Methods and Computerized Inversion of Data*, 20:243–257, 2004.

[13] F. Broggini and R. Snieder. Connection of scattering principles: A visual and mathematical tour. *European Journal of Physics*, 33:593–613, 2012.

[14] K. Wapenaar, P. Broggini, E. Slob, and R. Snieder. Three-dimensional single-sided Marchenko inverse scattering, data-driven focusing, Green's function retrieval, and their mutual relations. *Physical Review Letters*, 110:084301, 2013.

[15] K. Wapenaar, J. Thorbecke, J. van der Neut, F. Broggini, E. Slob, and R. Snieder. Green's function retrieval from reflection data, in absence of a receiver at the virtual source position. *Journal of The Acoustical Society of America*, 135:2847–2861, 2014.

[16] J.T. Fokkema and P.M. van den Berg. *Seismic Applications of Acoustic Reciprocity*. Elsevier, Amsterdam, 1993.

[17] S. Oppenheim, R.W. Schafer, and J.R. Buck. *Discrete-Time Signal Processing*. Prentice-Hall, New York, 1998.

[18] H. Ricker. The form and laws of propagation of seismic wavelets. *Geophysics*, 9:314–323, 1953.

[19] R. Snieder, M. Miyazawa, E. Slob, I. Vasconcelos, and K. Wapenaar. A comparison of strategies for seismic interferometry. *Surveys in Geophysics*, 30:503–523, 2009.

[20] K. Wapenaar, J. van der Neut, E. Ruigrok, D. Draganov, J. Hunziker, E. Slob, J. Thorbecke, and R. Snieder. Seismic interferometry by crosscorrelation and by mutidimensional deconvolution: A systematic comparison. *Geophysical Journal*, 185:1335–1364, 2011.

[21] J. van der Neut, J. Thorbecke, K. Mehta, E. Slob, and K. Wapenaar. Controlled-source interferometric redatuming by crosscorrelation and multidimensional deconvolution in elastic media. *Geophysics*, 76:SA63–SA76, 2011.

[22] K. Wapenaar, R. Snieder, S. de Ridder, and Slob. E. Green's functions representations for Marchenko imaging without up/down decomposition. *Geophysical Journal-oxford*, 227:184–203, 2021.

[23] H.J.S. Dorren, E.J. Muyzert, and R.K. Snieder. The stability of one-dimensional inverse scattering. k *Inverse Problems. An International Journal on the Theory and Practice of Inverse Problems, Inverse Methods and Computerized Inversion of Data*, 10:865–880, 1994.

[24] H.J.S. Dorren and R.K. Snieder. One-dimensional inverse scattering using data contaminated with errors. In H.V. von Geramb, editor, *Lectures Notes in Physics, Quantum Inversion Theory and Applications*, pages 405–411. Springer-Verlag, Berlin, 1994.

[25] F. Broggini, R. Snieder, and K. Wapenaar. Data-driven wavefield focusing and imaging with multidimensional deconvolution: Numerical examples from reflection data with internal multiples. *Geophysics*, 79:WA107–WA115, 2014.

[26] L. Diekmann, I. Vasconcelos, and T. van Leeuwen. A note on Marchenko-linearised full waveform inversion for imaging. *Geophysical Journal International*, 234(1):228–242, 2023.